

# THE LAMINAR-TURBULENT TRANSITION ZONE IN 2D AND 3D BOUNDARY LAYERS WITH EMPHASIS ON EFFECT OF FREE STREAM TURBULENCE

A.Ph. Kiselev\*, V.A. Kuzminsky\*, D.S. Sboev\*

\* Central aerohydrodynamic institute n.a. Prof. N.E. Zhukovsky (TsAGI),  
Zhukovsky, Russia

**Keywords:** *intermittency, transition prediction, swept wing, free stream turbulence*

## Abstract

*The present communication reports some recent findings on influence of intense free stream (FST) turbulence on boundary layer transition. Experimental investigation was conducted in TsAGI T-124 wind tunnel (WT). The distributions of intermittency over straight and swept wings models were used to specify the start and the end of transition zone.*

*Basing on the comparison with the experimental data, the possibilities of application of different methods for prediction of the FST-induced laminar-turbulent transition are analyzed.*

## 1 Introduction

The problem of laminar-turbulent transition in boundary layers is of greatest importance for the natural laminar flow technology. For its solution the developer's toolkit is desired which allows compute the characteristics of boundary layer disturbances initial amplitude and growth for determination of the laminar-turbulent transition location with sufficient accuracy. Thus the testing of boundary layer stability and laminar-turbulent transition prediction methods by comparison of calculation results and experimental data is necessary. Also, the influence on transition of various external disturbances by means of a receptivity processes needs to be more clarified in order to calibrate transition prediction methods for flight conditions as well as for various WTs.

Free-flight conditions for passenger aircrafts are characterized by large Reynolds

numbers and relatively low FST levels. While in free flight the turbulence level is as low as  $Tu = 0.07\%$  of the free-stream velocity, the industrial WTs have a FST levels ranging from 0.12-1.0%. The consequence of this is that transition to turbulence may take a different path as compared to free flight. To date some understanding of transition process under influence of elevated FST is achieved for 2D boundary layers (see [1], [2] for instance). On contrary, for 3D boundary layers the most investigations [3], [4] and [5] dealt with weak FST up to 0.3% (which is in range of world's most used industrial WTs) and very little known about influence on transition of moderate FST in range up to 1%. Only in [3], [4] some data were presented on transition process in 3D boundary layer with FST level up to 0.57%.

The proposed study is the continuation of the researches completed in TsAGI in the framework of the TELFONA project [6] (6<sup>th</sup> European FP). It is devoted to investigation of the possibilities to implement different engineering calculation methods to the laminar-turbulent transition prediction and the influence of higher FST level on its characteristics. To analyze these effects, the detailed experimental studies of transition zones on the straight and swept wings were carried out.

## 2 Experimental set-up and details of calculations

Experiments were performed in the TsAGI subsonic low-turbulence low-noise WT T-124. LV6 airfoil model is a rectangular wing with the

chord  $C = 1000$  mm and the span of 998 mm. This model was tested at zero incidence. The second model has been tested is the wing section model with the leading edge sweep angle  $\chi = 35^\circ$ , the chord length along the free stream direction 1000 mm and the span of 998 mm. This model has the same shape of the LV6 airfoil in the section along free stream direction. Regimes at angles of attack  $\alpha = -2^\circ$  and  $0$  were chosen for further investigations in swept wing boundary layer. Both models have the relative thickness of 11%. The experiments were conducted at free stream velocity  $U_0 = 80$  m/s that correspond to Reynolds number  $5.5 \times 10^6$  based on full chord of the model and Mach number 0.24. The system of coordinates was used with the longitudinal axis  $X$  directed perpendicularly to the leading edge of the wing, and the transversal axis  $Z$  directed along the leading edge.

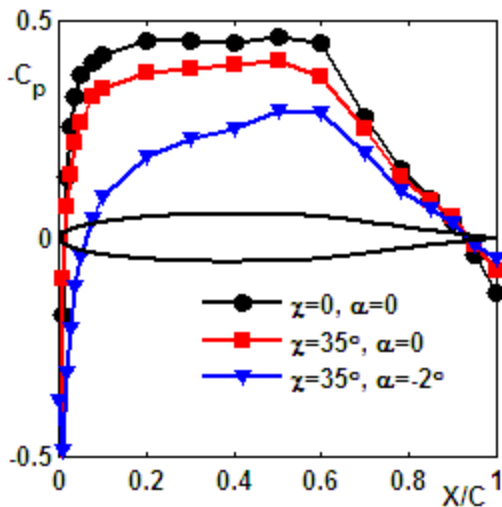


Fig. 1. Pressure distributions over the upper wing surface.

The pressure distributions over the models is given in Fig. 1. For both 2D and 3D cases at  $\alpha = 0$  the pressure distributions have the following specific features: after the domain of flow acceleration ( $X/C < 0.15$ ) there is a region practically without the pressure gradient. In this zero pressure gradient (ZPG) region the measured boundary layer velocity profiles coincide very well with Blasius solution for 2D case. On swept wing model there is favorable pressure gradient (FPG) region at  $\alpha = -2^\circ$ ,  $0 < X/C < 0.5$ .

The hardware component of the measuring system used consists of the single hot-wire with CTA DISA 55D01, a container for 32 pressure transducers, and an automatized traverse gear, which are connected to the PC through the input/output subsystem.

The experiments were carried out at three flow regimes: at the natural conditions of the WT test section and with the elevated FST level generated by two grids. Grids were installed at the point of entry to the test section. Turbulence level  $Tu_u$  (based on longitudinal component of pulsations  $u_{rms}$ ) at the model leading edge estimated by the values of 0.7% for grid G1 and 1.1% for grid G2. Turbulence level  $Tu$  (based on three components of pulsations) at the model leading edge estimated by the values of 0.61 % for grid G1 and 0.91 % for grid G2 due to some degree of anisotropy of generated turbulence ( $v_{rms}/u_{rms} = 0.73-78$ ). The Taylor micro-scale of turbulence for the longitudinal pulsations appeared to be equal to 5-6 mm for both grids. Longitudinal integral turbulence scale was made by means of integration of the autocorrelation function. For grid G1 the value of this scale was 21.3 mm and 44.7 mm for grid G2.

In all experiments the region of laminar flow destruction was determined by studying the intermittency  $\gamma$  in the boundary layer. The following model [7] for  $\gamma$  was used in the transition region

$$\gamma = 1 - \exp\left[-\frac{n\sigma}{U_0}(X - X_t)^2\right],$$

where  $X_t$  is the coordinate of the transition inception,  $n$  is the rate of turbulent spots generation in the domain of their emergence, and  $\sigma$  is a kinematic parameter depending on the velocity and angle of propagation of turbulent spots. It was demonstrated [7], [8] that this dependence can be used to describe transition regions in various flows. In particular, in the majority of flows, the function

$$F = \sqrt{-\ln(1-\gamma)}$$

in the transition region could be approximated by a straight lines. The crossings of these lines with

$X$  axis were chosen as  $X_t$  positions, while the value  $\gamma = 0.99$  ( $F = 2.14$ ) was chosen to specify transition completion position  $X_T$ . In order to characterize transition location with single parameter the position where  $\gamma = 0.5$  is referred below as  $X_{0.5}$ .  $\Delta X = X_T - X_t$  gives the length of transition region.

All intermittency measurements were performed at the height in the boundary layer corresponding to  $U/U_e = 0.5$ , i.e. in the middle of boundary layer ( $U_e$  is local external velocity). It allowed conducting the measurements in 3D boundary layer with single-wire probe, because the angles between direction of  $U_0$  and local inviscid streamline at this height in the measurements region didn't exceed  $2-4^\circ$  so resulting error didn't exceed 2%. The additional details of experimental techniques could be found in [9], [10].

The calculations of boundary layer were conducted using the algorithm based on finite-differences scheme of second order accuracy of approximation along longitudinal coordinate and fourth order accuracy along coordinate normal to the surface. In calculations the experimental pressure distributions were used.

General numerical matrix method for calculation of hydrodynamic stability characteristics of three-dimensional boundary layers developed in TsAGI was used. The computation of eigenvalues is performed for real counterpart of initial complex matrix with the use of QR-algorithm. For 2D flow the  $N$ -factors were computed using envelope method, while in 3D boundary layer cross-flow ( $N_{CF}$ ) and streamwise ( $N_{TS}$ , i.e. along inviscid streamline)  $N$ -factors were determined separately also with envelope method used as sub-strategy in both cases.

For transition prediction on the straight wing turbulence model of Langtry-Menter was used. Calculations were performed with the software package ANSYS CFX (TsAGI license No.501024) [11].

Despite a significant progress in the development of numerical methods, empirical and semi-empirical models of the transition are still widely used in engineering practice because of the high cost of large-scale numerical research. For 2D boundary layer at the elevated

FST levels the transition length was calculated using models by Mayle [8], Solomon *et al.* [12] and Roberts & Yaras [13]. Also in 3D case for low turbulence environment three simple empirical transition criteria were applied, namely, Arnal C1 [14], Brown [15], and Barinov–Lutovinov [16]. Finally, semi-empirical model recently developed by Ustinov [17] for FST-induced transition was tried. It based on transient growth idea with subsequent secondary instability of streaks.

### 3 The results

The all experimental and linear stability data sets discussed are summarized in the Table.

#### 3.1 2D boundary layer

The results of the measurements [9] demonstrated that at the natural conditions at  $X/C = 0.585$  there was a boundary layer separation with the creation of separation bubble in the  $X/C = 0.59-0.65$  zone. It was the region where transition took place.

The streamwise distributions of the intermittency function  $F$  are shown in Fig. 2 for the elevated FST cases. As measurements upstream of  $X/C = 0.12$  were impossible, the transition inception points were obtained by extrapolating the measured results in the upstream direction by means of approximating  $F(X/C)$  by straight lines. The laminar-turbulent transition began in both cases in the FPG region. It should be noted that these results agree very well with the measured evolution of the mean flow in the boundary layer [10].

As is seen from Fig. 2, the most detailed measurements of the dependence  $\gamma(X/C)$  could be performed in the G1 case. It was found that the dependence  $F(X/C)$  can be approximated by two straight lines with different slopes: a smaller one at the beginning of the measurement region and a larger further downstream. Narashima [7] termed this phenomenon “subtransition.” Let us recall that the FPG region on the LV6 model at a zero angle of attack extended down to  $X/C = 0.15$ , and further downstream it was replaced by ZPG region. Therefore, we can argue that the subtransition

Table

$(\alpha, \chi)$	Tu, %	$X_l/C$	$X_{0.5}/C$	$X_T/C$	$\Delta X/C$	$N_t$	$N_{0.5}$	$N_T$	comments
(0, 0)	0.064	0.594	0.615	0.648	0.054	13.46	-	-	laminar separation with turbulent reattachment
(0, 0)	0.61	0.055	<b>0.199</b>	0.319	<b>0.264</b>	0	3.05	7.06	bypass transition
(0, 0)	0.91	0.052	0.097	0.168	0.116	0	0.42	2.05	bypass transition
(0, 35°)	0.064	0.330	0.384	<b>0.468</b>	0.138	4.81 ( $N_{CF}$ ) 5.23 ( $N_{TS}$ )	5.02 ( $N_{CF}$ ) 6.59 ( $N_{TS}$ )	5.16 ( $N_{CF}$ ) 8.67 ( $N_{TS}$ )	strong interaction between TS- and CF-instabilities
(0, 35°)	0.61	0.108	<b>0.319</b>	<b>0.493</b>	<b>0.385</b>	2.72 ( $N_{CF}$ ) 0.21 ( $N_{TS}$ )	4.75 ( $N_{CF}$ ) 4.94 ( $N_{TS}$ )	5.16 ( $N_{CF}$ ) 9.51 ( $N_{TS}$ )	CF-instability and FST-induced streaks
(0, 35°)	0.91	0.077	0.152	0.271	0.194	1.84 ( $N_{CF}$ ) 0.01 ( $N_{TS}$ )	3.49 ( $N_{CF}$ ) 0.78 ( $N_{TS}$ )	4.47 ( $N_{CF}$ ) 3.63 ( $N_{TS}$ )	
(-2°, 35°)	0.064	0.146	0.314	0.391	0.245	7.67 ( $N_{CF}$ ) 0 ( $N_{TS}$ )	11.07 ( $N_{CF}$ ) 1.21 ( $N_{TS}$ )	12.01 ( $N_{CF}$ ) 2.21 ( $N_{TS}$ )	CF-instability
(-2°, 35°)	0.61	0.090	0.153	0.253	0.163	5.62 ( $N_{CF}$ ) 0 ( $N_{TS}$ )	7.88 ( $N_{CF}$ ) 0 ( $N_{TS}$ )	10.09 ( $N_{CF}$ ) 0.52 ( $N_{TS}$ )	
(-2°, 35°)	0.91	0.066	0.129	0.228	0.162	4.44 ( $N_{CF}$ ) 0 ( $N_{TS}$ )	7.13 ( $N_{CF}$ ) 0 ( $N_{TS}$ )	9.62 ( $N_{CF}$ ) 0.31 ( $N_{TS}$ )	

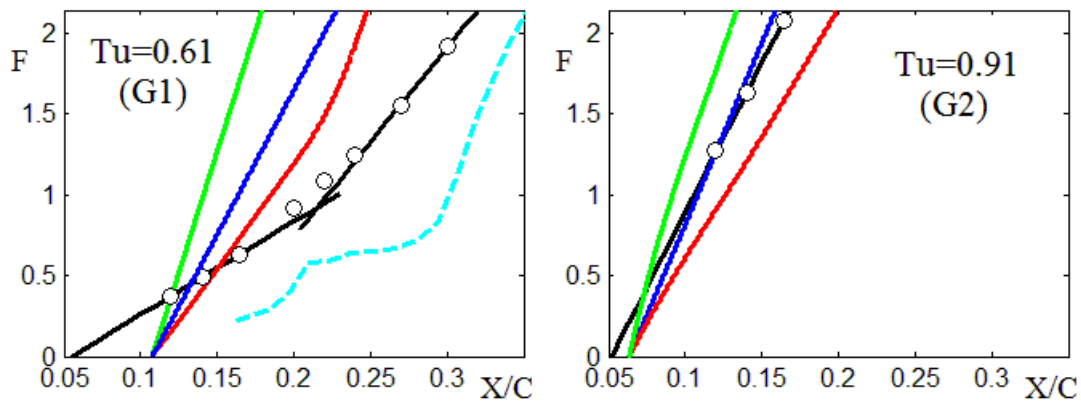


Fig. 2. Streamwise distributions of the intermittency for 2D boundary layer. The black lines are approximations of experimental data by straights, color solid curves are calculations by the model [8] (blue), [12] (red) and [13] (green). Dashed line is predictions of Langtry-Menter turbulence model (courtesy to Dr. Valery Vozhdaev [11]).

effect observed in this work is related to the influence of the pressure gradient distribution. In the case G2, the subtransition effect was not observed in our experiments, which was probably caused by the above-mentioned upstream constraint of the measurement region.

Mack [18] proposed the following empirical dependence of the  $N$ -factor on  $Tu$  for determining the point of the laminar-turbulent transition in the range  $0.1\% < Tu < 1\%$  on the basis of calculations of the linear theory of hydrodynamic stability:

$$N_{tr} = -8.43 - 2.4 \ln(Tu)$$

The values of the  $N$ -factor for the characteristic points  $X_l/C$  and  $X_T/C$  are shown in the Table. In G1 and G2 cases, the  $N$ -factors corresponding to  $X_l/C$  are equal to zero, i.e., the transition started in these situations before the boundary layer lost its stability (by-pass transition). The values of the  $N$ -factor are compared in Fig. 3 with the predictions. In the case G2, correlation overpredicts the  $N$ -factor of the transition. At  $Tu = 0.61\%$ , the criterion yields feasible results, especially if the value corresponding to the  $X_{0.5}/C$  is treated as the transition point. This is consistent with the V.S. Kosorygin's data [19].

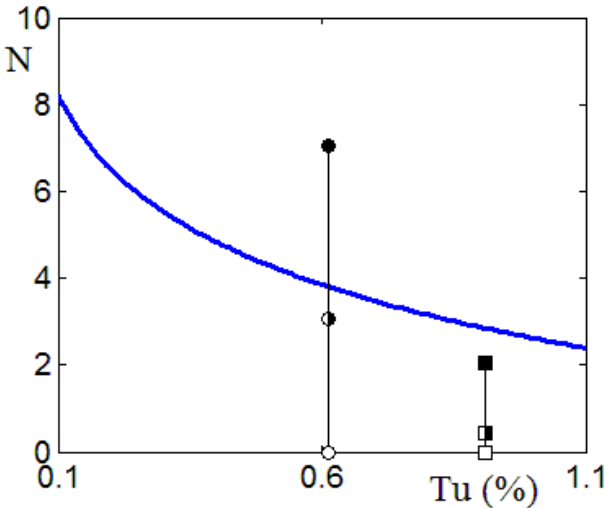


Fig. 3. Dependence of the transition  $N$ -factor on the FST level for 2D flow. The solid line shows the Mack relation, open symbols corresponds to the  $X_l$ , solid symbols to the  $X_T$ , the half-open symbols refers to the  $X_{0.5}$ .

The value of  $X_l$  is also was determined by using empirical relations. When the experimental data were compared with these correlations, it turned out that the correlations [20], [21] predict too high values for the Reynolds number of the transition inception based on the momentum thickness (it should be noted that correlation [21] gives value of  $Re_\theta$  at the  $\gamma = 0.1$  position). The best estimates were obtained by the well known correlation by Mayle [8]:

$$Re_{\theta t} = 400 Tu_u^{-5/8}, \quad Re_\theta = U_\epsilon \theta / \nu$$

As is seen from Fig. 2, this correlation ensures fairly reasonable results for  $X_l/C$  (0.108 and 0.064 for G1 and G2, respectively), though they are slightly shifted downstream from the experimental data. It should be noted that correlations [20], [21] were obtained on flat plates with small leading edge radii, while Mayle's correlation based on more broad set of data. The LV6 airfoil has thicker leading edge with radius 21.8 mm. It is shown in [22], that an increase in the leading edge radius shifts the transition point upstream in flows with elevated FST. The present findings are in accordance with it.

The transition length was calculated by the models [8], [12] and [13]. The calculated results are plotted in Fig. 2. From the comparison of these results with experimental data, we can see that the best results in terms of both the transition zone length and the rate of generation of turbulent spots and characteristics of their propagation (these quantities are proportional to the slope of the calculated curves in the figure) are provided by the model [12], which takes into account the dependence of these quantities on the pressure gradient and predicts the subtransition effect. The correlation [8] with a constant rate of generation of turbulent spots also gives good results. It should be noted that all examined correlations underpredict the transition zone length.

Function  $F$  is presented as follows in [17]:

$$F = A^{1/2} (Re_x)^{1/4} \left( \frac{u'_{lam}}{U_0 a_c} \right)^2 \exp \left[ -\frac{1}{4} \left( \frac{U_0 a_c}{u'_{lam}} \right)^2 \right]$$

where  $u'_{lam}$  is rms amplitude of the velocity pulsations at the laminar flow zones,  $A$  and  $a_c$  are constants. When the measured parameters  $F$  and  $u'_{lam}$  are known, these constants may be defined by means of linear approximation from the expression

$$G = \ln\left(\frac{U_0^4 F^2}{u'_{lam}{}^4 Re_X^{1/2}}\right) = -\frac{1}{2} a_c^2 \left(\frac{U_0}{u'_{lam}}\right)^2 + \ln\left(\frac{A}{a_c^4}\right)$$

The relations  $u'_{lam}(X)$  were defined for all cases under investigation. Along with the data on  $\gamma$ , these relations were used to define constants  $A$  and  $a_c$ . It appeared that in most cases the definition of the necessary constants from the test data is impossible because the relation of  $G$  vs. inverse square  $u'_{lam}$  can't be represented as a linear function. Moreover, sometimes function  $G$  was the increasing but not the decreasing one. Probably such a behavior took place because of high intermittency values  $\gamma > 0.1$ , which were observed in the most part of the investigated test cases from the very beginning of the measured area. The work is being done now on checking the theory [17] in the 2D boundary layer at lower Reynolds numbers.

Fig. 2 also demonstrates predicted by Langtry-Menter model distributions of  $\gamma$  in G1 case. For modelling of the turbulizing grid at the entrance to the computational domain the boundary condition included turbulence intensity 0.61% and turbulent-to-molecular viscosity ratio  $\mu/\mu_t = 100$ . Satisfactory accuracy of the Lantry-Menter model for this type of flow may be noticed. In particular, the subtransition effect is clearly seen and transition completion is predicted with accuracy about 5% of  $C$ . Attempts to simulate the flow at higher turbulence level (G2 case) were not successful.

### 3.2 3D boundary layer

Fig. 4 shows computed dependencies of  $N$ -factors on streamwise coordinate for swept wing. In Fig. 5 the measured distributions of intermittency through transition region are given for all cases under consideration. It is seen from Fig. 4 that in  $\alpha = -2^\circ$  case the cross-flow (CF)

$N$ -factor ( $N_{CF}$ ) has much higher values than streamwise  $N$ -factor ( $N_{TS}$ ). At natural conditions the CF-instability dominates transition and formation of stationary vortices in the boundary layer was observed in experiment in this case. As pressure distribution changes to FPG-ZPG combination in  $\alpha = 0$  regime, the values of  $N$ -factors reflects this with sharp increasing of  $N_{TS}$  to 10 and decreasing of  $N_{CF}$  to nearly 5 at the end of measurements region. In this case a system of stationary CF-vortices was also observed in boundary layer at natural conditions. However, the values of  $N$ -factors in characteristic points through transition region (see Table) shows that strong interaction between CF- and streamwise instabilities exists in this regime (for  $\alpha = -2^\circ$  and 0 at  $X_{0.5}/C$  point increasing of  $N_{TS}$  from 1.2 to 6.6 reduces  $N_{CF}$  from 11 to 5).

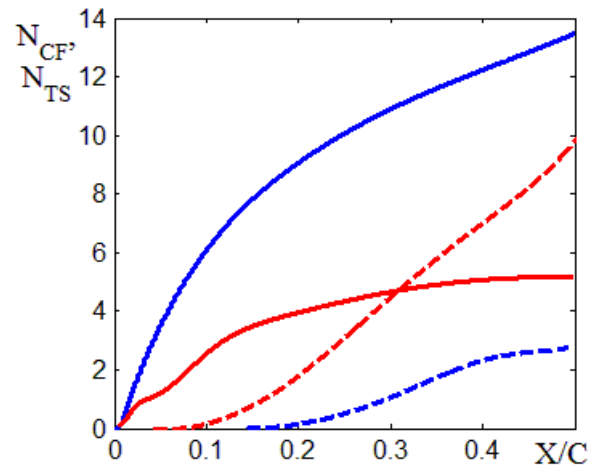


Fig. 4.  $N$ -factors dependence from the longitudinal coordinate for the swept wing model. The  $N_{CF}$  and  $N_{TS}$  are shown by solid and dashed lines respectively. Blue and red lines corresponds to  $\alpha = -2^\circ$  and 0 respectively.

The empirical criteria, allowing to estimate the transition location on the swept wings basing only on the averaged flow characteristics, are widely used in the engineering practice [14], [15] and [16]. Basing on the criteria [15], [16] it is possible to define the Reynolds number of the cross-flow instability  $Re_{CF}^*$ . Local Reynolds number  $Re_{0.1}$  is calculated using the maximum value of the cross-flow  $W_{max}$  in the coordinate system associated with the inviscid streamline, and the distance from the surface  $Y_{0.1}$ , where

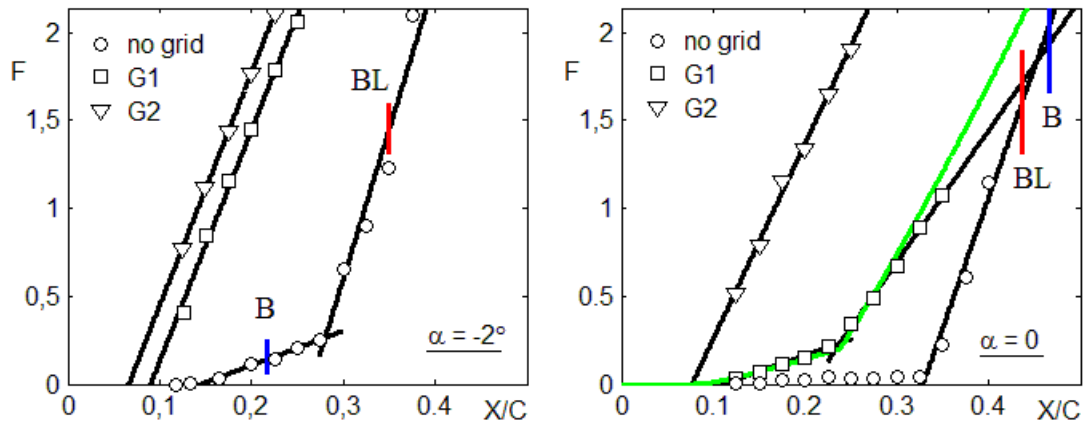


Fig. 5. Streamwise distributions of the intermittency for 3D boundary layer,  $\alpha = -2^\circ$  (left) and 0 (right). The black lines are approximations of experimental data by straights; blue and red lines shows transition locations defined by Brown criterion (B, [15]) and Barinov-Lutovinov criterion (BL, [16]). Intermittency distribution for G1 case calculated using [17] is shown by green.

cross flow reduces to the value of  $0.1W_{\max}$ . It is considered that transition takes place when the ratio  $Re_{0.1}/Re_{CF}^*$  exceeds certain value  $K_{CF}$ . According to the results of [23] the value  $K_{CF}$  was taken to be equal to 3.

The results of implementation of these criteria for definition of the transition location in the natural conditions (low FST level) are shown in Fig. 5. The C1 criterion [14] at  $\alpha = -2^\circ$  gives too downstream shifted transition location, and at  $\alpha = 0$  this criterion predicts absence of transition up to the separation line in the adverse pressure gradient zone. Criterion [15] has scatter of about 10% of  $C$  relative to  $\gamma = 0.5$  point in both positive and negative. The best results were demonstrated by the criterion of Barinov and Lutovinov [16], which in both cases predicts the transition location shifted downstream from the point  $\gamma = 0.5$  by approximately 5% of the chord, i.e. corresponding to  $\gamma \approx 0.8$  ( $F \approx 1.5$ ).

From the Fig. 5 it is seen that the "subtransition" effect is also observed in 3D boundary layer for both angles of attack. This effect is linked with the reasonably fast changes in pressure distribution over the model.

The influence of elevated FST level at  $\alpha = -2^\circ$  manifests itself by upstream shifting of transition inception locations with increasing of  $Tu$ . In this case, as it was mentioned earlier, the pure CF-instability dominates transition in low disturbed environment. However, the slopes of

the  $F$  distributions remains unchanged with increasing of  $Tu$  from 0.61 to 0.91% (see left plot in Fig. 5). Consequently, the turbulent spots production rate is almost independent on FST level in this regime.

Much more complicated situation takes place at  $\alpha = 0$ . From the comparison of data shown in Fig. 2 and 5 and in the Table, it can be seen that the values of  $X_i$  and  $X_T$  are higher at the elevated FST level on the swept wing than on the straight wing at the same values of  $Tu$ . In addition, the slopes of lines  $F(X)$  on the swept wing is lesser than on the straight wing. Taking into account that there is ZPG region at  $X/C > 0.2$  on both models, it is possible to conclude that the turbulent spots production rate on the swept wing is lower than on the straight wing at an identical FST level. For  $Tu = 0.61\%$ , the characteristic values of  $\Delta X/C = 0.39$  and  $X_{0.5}/C = 0.32$  are obtained on the swept wing, while they are 0.26 and 0.2, respectively, on the straight wing. The same effect also takes place at  $Tu = 0.91\%$ . It means that, at some combination of FST level and pressure distribution, a transition location on the swept wing could move downstream in comparison to the straight wing with the same cross-section and at the same angle of attack. As opposed to this, at natural conditions of the WT test section the measured values of  $X_{0.5}/C$  at  $\alpha = 0$  is 0.62 and 0.38 for the straight and swept wing respectively - well known result due to high

increments of inviscid CF-instability. Another uncommon feature is revealed by comparison of intermittency distributions with  $Tu=0.064$  and  $0.61\%$  at  $\alpha=0$ . It seen from the Fig. 5 and the Table that at increased FST level the transition takes longer distance from its inception and completes even downstream that at low FST ( $X_T/C = 0.47$  and  $0.49$ ).

The observed features of the transition under conditions of the increased FST on a swept wing at  $\alpha=0$  could be connected to the pronounced presence of disturbances of different types in the boundary layer in addition to the unstable cross-flow disturbances. In Fig. 6 the spanwise distribution of wall temperature fluctuations  $T'_w$  is shown together with its spanwise wavelength spectrum. These data were measured by means liquid-crystal coating. The observed dominant wavelength corresponds to 4-6 boundary layer thickness and agrees very well with the wavelength of CF-vortices. Also the packet of traveling CF-modes with central frequency that agrees with computed most unstable frequencies was detected in hot-wire signal (Fig. 7). However, the most amplified disturbances in this case are low-frequency (below 100 Hz) disturbances, so called "streaky structures" excited by the localized vortical disturbances of the external flow in both the 2D and 3D boundary layers [24]. Developed in the boundary layer, the streaks, localized in space and time, results in the occurrence of turbulent spots also localized in space and time. The streaks and the incipient turbulent spots at different stages of development were seen clearly in hot-wire traces. Some examples are shown in Fig. 8. It's important to notice that growth of fluctuations on a laminar parts of flow  $u'_{lam}$  is proportional to square root of  $X$  as shown in Fig. 9, where distribution of  $u'_{lam}$  is approximated by two parabolas (the changes in pressure distribution leads to the changes in coefficients of polynomial). It's compares very favorably with the results of transient growth theory.

Therefore, under the conditions of this experiment at the elevated FST, the dynamics of destruction zone of the laminar flow in the boundary layer was determined by the arising and the subsequent merging of turbulent spots

excited by the external turbulence instead by the development of instability of the average velocity profiles in boundary layer.

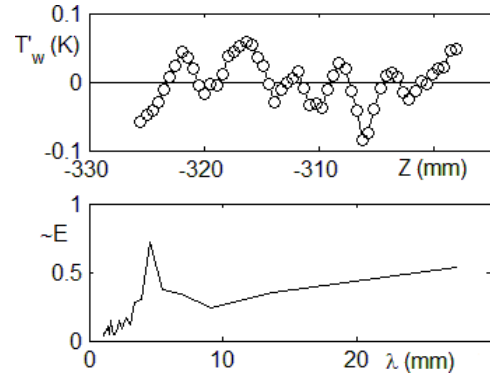


Fig. 6. The spanwise distribution of wall temperature fluctuations and its wavelength spectrum,  $\alpha=0$ ,  $\chi=35^\circ$ ,  $Tu=0.61\%$ ,  $X/C=0.2$ .

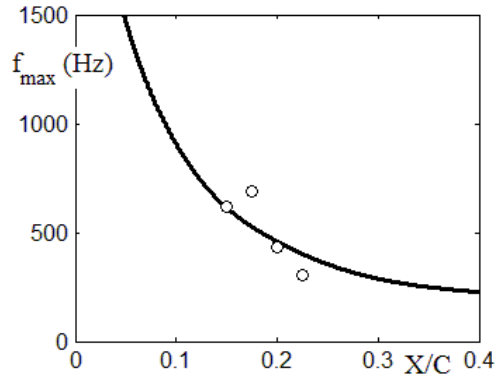


Fig. 7. The computed most unstable frequencies of CF-modes in comparison with the experiment,  $\alpha=0$ ,  $\chi=35^\circ$ ,  $Tu=0.61\%$ .

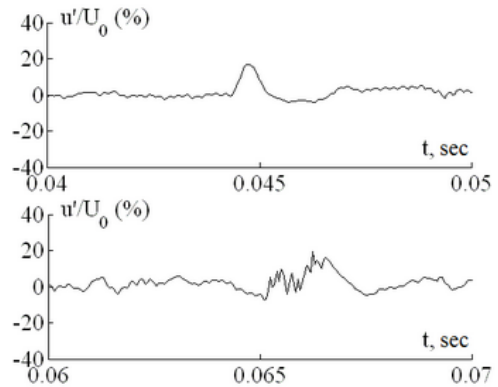


Fig. 8. The low-frequency streak (upper trace) and young spot (lower trace) in hot-wire signal,  $\alpha=0$ ,  $\chi=35^\circ$ ,  $Tu=0.61\%$ ,  $X/C=0.175$ .

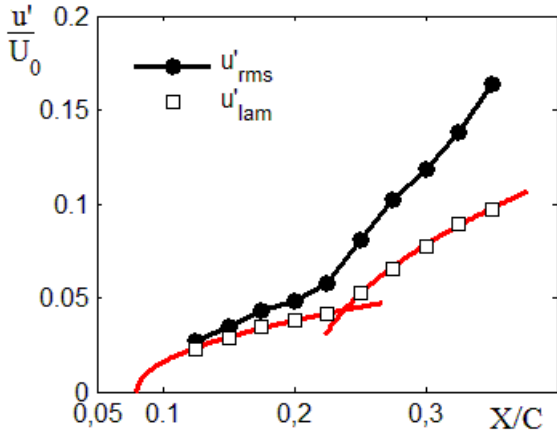


Fig. 9. The streamwise distributions of rms fluctuations and fluctuations at the laminar flow zones  $u'_{lam}$ ,  $\alpha = 0$ ,  $\chi = 35^\circ$ ,  $Tu = 0.61\%$ .

For this case ( $\alpha = 0$ ,  $\chi = 35^\circ$ ,  $Tu = 0.61\%$ ) it became possible to define constants  $A$  and  $a_c$  in the model of intermittency [17]. The  $u'_{lam}(X)$  relation for this case is shown in Fig. 9. The test points were approximated with two polynomials of the  $X^{1/2}$  type, also shown in the figure. These relations along with the constants  $A$  and  $a_c$  were used for calculation of function  $F$ . Fig. 5 demonstrate the result of calculation compared with the experimental data. A very good agreement is seen in the  $X/C < 0.3$  zone and a satisfactory one downstream from it. The predicted relation  $F(X)$  is not smooth because the non-smooth  $u'_{lam}(X)$  dependence was used in calculations. As it follows from Fig. 5, the theory [17] describe the “subtransition” effect correctly basing only on the dependence between the  $u'_{lam}(X)$  grows and the longitudinal pressure gradient without any additional hypotheses concerning the turbulent spots development changes as it was done in the theories [7], [12] and [13]. When the external turbulence excite the streaks, the  $u'_{lam}(X)$  relation may be predicted for different boundary layers using transient growth approach. The values of  $X_{0.5}/C$  and  $X_7/C$  achieved by means of the  $F(X)$  dependence, calculated using model [17], were 0.311 and 0.443 correspondingly and coincided with the table ones with the accuracy of 1–5% of the chord.

Inspite of good agreement between the experimental and calculated  $F(X)$  dependencies, there exist substantial discrepancies between the

results of this study and [17]. So, the  $A$  and  $a_c$  constants in this work appeared equal to  $10^{-5}$  and 0.03 respectively. These values are in sharp contrast with the achieved in [17] ones  $A = 10.4$  and  $a_c = 0.34$  for the 2D ZPG boundary layer. Further investigations in this direction are necessary because basing on [17] a rather effective semi-empirical method of the boundary layer transition prediction may be created for the conditions of elevated FST.

#### 4 Conclusions

The important findings to practice of this study could be summarized as following:

- The empirical and semi-empirical models, allowing to estimate the transition location basing only on the averaged flow characteristics are still very robust and effective means for laminar-turbulent transition prediction at elevated FST level, at least in 2D boundary layers.
- The leading edge geometry is very important in a FST-induced boundary layer transition. The increasing of leading edge radius promotes transition upstream even in ZPG boundary layer.
- In 3D boundary layers at some specific combinations of the pressure distribution and FST-level the very uncommon ways to transition could be existing. This fact must be accounted for careful planning of experiments in industrial wind tunnels.

#### References

- [1] Boiko AV, Dovgal AV, Grek GR and Kozlov VV. *The origin of turbulence in near-wall Flows*. Springer Science & Business Media, 2002.
- [2] Durbin P and Wu X. Transition beneath vortical disturbances. *Annual Review of Fluid Mechanics*, Vol. 39, pp 107-128, 2007.
- [3] Deyhle H and Bippes H. Disturbance growth in an unstable three-dimensional boundary layer and its dependence on environmental conditions. *Journal of Fluid Mechanics*, Vol. 316, pp 73-113, 1996.
- [4] Kurian T, Jens H. M. Fransson JHM and Alfredsson PH. Boundary layer receptivity to free-stream

- turbulence and surface roughness over a swept flat plate. *Physics of Fluids*, Vol. 23, No. 1, pp 034107-1 - 034107-13, 2011.
- [5] Downs RS and White EB. Free-stream turbulence and the development of cross-flow disturbances. *Journal of Fluid Mechanics*, Vol. 735, pp 347-380, 2013.
- [6] Chernyshev SL, Ivanov AI, Kiselev APh, Kuzminsky VA, Sboev DS and Zhigulev SV. Experimental and numerical investigation of the laminar-turbulent transition mechanisms in the boundary layer on 2D and 2.5D models in the low-turbulence wind tunnel. *Proc 5-th European Conference on Computational Fluid Dynamics (ECCOMAS CFD 2010)*, Lisbon, Portugal, paper No. 1786, 2010.
- [7] Narasimha R. The laminar-turbulent transition zone in the boundary layer. *Progress in Aerospace Sciences*, Vol. 22, No. 1, pp 29-80, 1985.
- [8] Mayle RE. The role of laminar-turbulent transition in gas turbine engines. *Journal of Turbomachinery*, Vol. 113, No. 4, pp 509-537, 1991.
- [9] Vlasov VA, Zhigulev SV, Ivanov AI, Kiselev APh, Kuzminsky VA, Sboev DS and Chernyshev SL. Laminar-turbulent transition on the LV6 laminarized airfoil: natural transition. *TsAGI Science Journal*, Vol. 42, No. 5, pp 565-591, 2011.
- [10] Vlasov VA, Zhigulev SV, Ivanov AI, Kiselev APh, Kuzminsky VA, Sboev DS and Chernyshev SL. Laminar-turbulent transition on the LV6 laminarized airfoil. Part II: effect of free stream disturbances. *TsAGI Science Journal*, Vol. 42, No. 6, pp 729-756, 2011.
- [11] Vozhdaev VV, Kiselev APh, Sboev DS, Teperin LL and Chernyshev SL. Numerical modeling of the position of a laminar-turbulent transition on a wing with the laminar airfoil LV6. *TsAGI Science Journal*, Vol. 44, No. 1, pp 65-76, 2013.
- [12] Solomon WJ, Walker GJ and Gostelow JP. Transition length prediction for flows with rapidly changing pressure gradients. *Journal of Turbomachinery*, Vol. 118, No. 4, pp 744-751, 1996.
- [13] Roberts SK and Yaras MI. Modeling transition in separated and attached boundary layers. *Journal of Turbomachinery*, Vol. 127, No. 2, pp 402-411, 2005.
- [14] Arnal D, Habiballah M and Coustols C. Laminar instability theory and transition criteria in two- and three-dimensional flows. *La Recherche Aéronautique*, No. 2, pp 125-143, 1984.
- [15] Brown WB. A stability criterion for three-dimensional laminar boundary layers. in *Boundary layer and flow control. Vol. 2*. Pergamon Press, 1961. pp 913-923.
- [16] Barinov VA and Lutovinov VM. On the parameters of approximate relationship of critical Reynolds number in the three-dimensional boundary layer. *Uchenye Zapiski TsAGI*, Vol. 4, No. 4, pp 27-32, 1973 (in Russian).
- [17] Usinov MV. Statistical description of laminar-turbulent transition in a boundary layer at high freestream turbulence degree. *Fluid Dynamics*, Vol. 48, No. 2, pp 192-200, 2013.
- [18] Mack LM. Transition prediction and linear stability theory. in *AGARD CP-224*. 1977. pp 11-22.
- [19] Crouch JD. Modeling transition physics for laminar flow control. AIAA Paper 2008-3832. 2008.
- [20] Abu-Ghannam BJ and Shaw R. Natural transition of boundary layers: the effects of turbulence, pressure gradient and flow history. *Journal Mechanical Engineering Science*, Vol. 22, No. 5, pp 213-228, 1980.
- [21] Fransson JHM, Matsubara M and Alfredsson PH. Transition induced by free-stream turbulence. *Journal of Fluid Mechanics*, Vol. 527, pp 1-25, 2005.
- [22] Zhigulev SV, Uspensky AA and Ustinov MV. Effect of the freestream turbulence scale and the leading edge shape on boundary layer laminar-turbulent transition. *Fluid Dynamics*, Vol. 44, No. 1, pp 31-44, 2009.
- [23] Kiselev APh and Bokser VD. Investigation of flow laminarization of swept wings. in *TsAGI—principal stages of scientific activities 1993—2003*. Nauka-Fizmatlit, 2003. pp 133-138 (in Russian).
- [24] Grek HR, Kozlov VV and Sboev DS. Receptivity of a Boundary Layer to a Localized Free Stream Disturbance. *Proc Laminar-Turbulent Transition: IUTAM Symposium*, Sedona, Arizona, pp 131-136, 1999.

### Contact Author Email Address

mailto: t124@inbox.ru

### Copyright Statement

The authors confirm that they, and/or their company or organization, hold copyright on all of the original material included in this paper. The authors also confirm that they have obtained permission, from the copyright holder of any third party material included in this paper, to publish it as part of their paper. The authors confirm that they give permission, or have obtained permission from the copyright holder of this paper, for the publication and distribution of this paper as part of the ICAS 2014 proceedings or as individual off-prints from the proceedings.